Supplementary Information

Morphology-Controlled Fully Spray-Coated Organic Solar Cells with High Power-to-Weight Ratio

Qin Wang[1], Kang An[1,*], Zhisheng Zhou[1], Hongyu Zhang[1], Zhipeng Yin[1], Jialin Wu[1], Xingwang Kang[1], Feiyue Lu[1], Xujie Hui[1], Wei Meng[1], Youyu Jiang[2], Yinhua Zhou[2], Keyou Yan[3], Lei Ying[1], Ning Li[1,4*]

[1] *Institute of Polymer Optoelectronic Materials & Devices, Guangdong Basic Research Center of Excellence for Energy and Information Polymer Materials, State Key Laboratory of Luminescent Materials & Devices, South China University of Technology, Guangzhou 510640, China.*

[2] *Wuhan National Laboratory for Optoelectronics, Huazhong University of Science and Technology, Wuhan 430074, China*

[3] *School of Environment and Energy, Guangdong Provincial Key Laboratory of Solid Wastes Pollution Control and Recycling, State Key Laboratory of Luminescent Materials & Devices, South China University of Technology, Guangzhou 510640, China.*

[4] *Guangdong Provincial Key Laboratory of Luminescence from Molecular Aggregates, South China University of Technology, Guangzhou, China.*

E-mail: *mskangan@scut.edu.cn*; *ningli2022@scut.edu.cn*

Keywords: morphology optimization, spray coating, organic solar cells, power-to-weight ratio

Experimental Procedures

Materials:

The aqueous dispersion of poly(3,4-ethylenedioxythiophene)-poly(styrenesulfonate) (PEDOT:PSS, PVP Al 4083) was purchased from Heraeus. D18, L8BO and PFN-Br were purchased from Dongguan Volt-Amp Optoelectronics Technology Company, Ltd. Polymer PYIT were purchased from Organtec Ltd. Silver nanowires were purchased from Zhejiang Kechuang Advanced Materials Technology Company, Ltd. PEDOT:F was synthesized by the Yinhua Zhou group. ZnO nanoparticles (N10 5 WT%) were purchased from Avantama and diluted to 0.2 WT% before use. Other materials were used as received without further purification unless otherwise stated. All solvents were ordered from Sigma-Aldrich.

Device Fabrications:

The device structure of conventional organic solar cells (OSCs) is ITO/PEDOT:PSS/Active Layer/PFN-Br/Ag, and the device structure of inverted organic solar cells is ITO/ZnO/Active Layer/PEDOT:F/Ag. The indium tin oxide (ITO) substrates were cleaned by sequential sonication for 30 min with detergent, deionized water, and isopropyl alcohol. After drying in an oven at 70 °C overnight, the substrates were treated with oxygen plasma for 2 min befor uesd. For conventional organic solar cells, a PEDOT:PSS (4083) hole transport layer of approximately 35 nm was spin-coated onto the ITO substrate at 3000 rpm for 30 seconds. The samples were thermally annealed on a hot plate at 150 ℃ for 20 min in an air atmosphere. For active layer, the deposition process employed a U-STAR KP-35 spray gun in combination with a UA-604G mini air compressor. During the spraying process, the nozzle positioned approximately 4 cm from the surface of the substrate. The handheld spray gun was moved along a uniform linear reciprocating path parallel to the substrate surface, at a spraying speed of approximately 0.5 cm s^{-1}. The spray path covered the entire active area of the substrate to ensure homogeneous film formation. Both the substrate temperature and environmental humidity were kept consistent with ambient conditions during spray deposition. The substrate temperature was maintained at approximately 25 ℃, and the relative humidity was controlled at around 50% RH via a constant-temperature and constant-humidity system, ensuring stable solvent evaporation and film-formation kinetics. The weight ratio of D18:PYIT and D18:L8BO were 1:1.2 and

the optimized weight ratio of D18:L8BO:PYIT was 1:0.8:0.4, with the concentration of polymer donor was 1 mg mL^{-1} in Tol solution. The spray solution dissolved on a hot plate at 130 °C for more than 2 h. The optimized spray setup air pressure was 19 psi. The thickness of active layers was controlled with the solution volume of 115 μL, corresponding time about 30 seconds. Spray-coated D18:L8BO:PYIT film was then transferred into a N_2 filled glove box to perform solvent vapor annealing (SVA) treatment. A homemade glass platform (20 mm × 20 mm, 10 mm high) was placed in the center of a 60 mm glass Petri dish to support the 15 mm × 15 mm ITO substrate. Then, 2 μL of CF was added without submerging the platform, and the covered dish was kept at ~20 ℃ to allow the vapor to fill the enclosed space. The film was then treated for the desired duration and allowed to stand for 5 min before subsequent processing (Figure S4, Supplementary Information). All films were thermal annealing on a 115 ℃ hot plate for 20 minutes. A PFN-Br electron transport layer of approximately 5 nm was spin-coated onto the BHJ at 2500 rpm, with a PFN-Br concentration of 0.5 mg mL^{-1} dissolved in methanol. For inverted organic solar cells, after 2 min of oxygen plasma treatment, a ZnO electron transport layer was spin-coated onto the ITO substrate at 2000 rpm for 30 s. The samples were thermally annealed on a hot plate at 100 °C for 10 min in an air atmosphere. The active layer was prepared using the same method as for conventional organic solar cells. PEDOT:F was spin-coated onto the BHJ at 3000 rpm for 30 s. Finally, a 105 nm Ag was thermally evaporated on top of the interface through a shading mask in a vacuum chamber at a pressure of 1×10^{-7} mbar. The effective area of the device was defined as 0.0516 cm^2, which was further limited to 0.04 cm^2 by a non-refractive mask to improve the measurement accuracy. For fully-sprayed high Power-to-Weight Ratio Organic Solar Cells, the structure is AgNWs@ZnO/ZnO/D18:L8BO:PYIT/PEDOT:F/AgNWs. For the bottom electrode (AgNWs@ZnO), 1wt% of the original AgNWs solution was diluted with ethanol at a ratio of 1:3. ZnO nanoparticles (N10 5 wt%) were diluted to 0.5 wt% in ethanol. The two components were then thoroughly mixed in a volume ratio of 2:1 before use. For the electron transport layer, the ZnO nanoparticles were diluted to 0.2 wt% in ethanol. The PEDOT:F was subjected to ultrasonic vibration for 1 minute prior to direct use. For the top electrode (AgNWs), the 1 wt% stock solution of AgNWs was diluted to 0.25 wt% in ethanol before application. The spraying processing for all functional layers followed the aforementioned procedures. The volumes used for

AgNWs@ZnO, ZnO, PEDOT:F and AgNWs were 80 μL, 40 μL, 55 μL and 300 μL, respectively. All spraying processes were conducted in an ambient atmosphere.

Instruments and measurement:

J-V measurement

The *J-V* curves were measured on a computer-controlled Keithley 2400 source meter under 1 sun, AM1.5 G spectra from the solar simulator (Enlitech), the light intensity was 100 mW cm^{-2} as calibrated by using a China General Certification Centre (CGC) certified reference monocrystal silicon cell (Enlitech). Before the *J-V* test of small area devices, a physical mask containing an aperture with a precise area of 4 mm^2 was used to define the device area.

Light-intensity dependence measurement

The light-intensity dependence measurements were carried out with illumination between 3-100 mW cm^{-2}, which was calibrated by a filter with designed optical densities between the samples and the light source and calibrated by the NIM-certified silicon reference cell. The current density and voltage were recorded with a Keithley 2400 source meters. The light-intensity dependence of V_{OC} is described by

$$V_{OC} \propto n\frac{k_B T}{q}\ln P_{light}$$

where n, q, T and k_B represent the indicator of trap-assisted recombination, elementary charge, temperature, and Boltzmann constant, respectively. The light-intensity dependence of J_{SC} is described by $J_{SC} \propto {P_{light}}^{\alpha}$ where α is exponential factor.[1]

J_{ph}-V_{eff} measurement

J_{ph} is defined as $J_{ph} = J_L - J_D$, where J_L and J_D are the current densities under light illumination and in the dark, respectively. V_{eff} is defined as $V_{eff} = V_0 - V_a$, where V_0 is the voltage at $J_{ph} = 0$, and V a is the applied voltage. J_{sat} is the saturation photocurrent density at high value of V_{eff} and the exciton dissociation probability (P_{diss}) is calculated by $P_{diss} = J_{ph} / J_{sat}$ at short-circuit condition.

EQE, UV-vis spectra and In-situ absorption spectra

Quantum efficiency measurement system QE-R3011 (Enlitech) was used to record the EQE data for all samples. The light intensity is calibrated by a standard single-crystal silicon photovoltaic cell (Enlitech). The UV-vis-NIR transimttance spectra of the AgNWs@ZnO, absorption spectra of the pure and mixed films were recorded on the QE65Pro spectrometer which is produced by Ocean Optics. In-situ absorption spectra were obtained using a QE Pro spectrometer (Ocean Optics).

AFM measurement

AFM images were acquired using a Bruker Multimode 8 microscope in tapping mode.

TRPL, Sheet resistance and stability measurement

The time-resolved photoluminescence (TRPL) spectra was obtained with the Germany PicoQuant fluorescence spectrometer (FluoTime 300). The sheet resistance of the botttom electrode AgNWs@ZnO was measured using the RTS-8 four-probe tester. For the light aging test, a set of white LEDs (spectral range: 400-800 nm, Wuhan 91PVKSolar) was used as the light source. The light intensity was equivalent to one sun and calibrated to ensure the generated photocurrent matched that of the solar simulator. The device under test was continuously aged by connecting a fixed 500-ohm resistor in series.

Device simulation model

In the single-junction solar cell device, the equivalent circuit includes a current source I_L, a diode I_D, a shunt resistor R_{sh} connected in parallel, and a series resistor R_s connected in series with them. The circuit current can be expressed as the following formula:

$$I = I_L - I_0\left[\exp\left(\frac{q(V+IR_s)}{nkT}\right)-1\right]-\frac{V+IR_s}{R_{sh}} \#(1)$$

where I, I_{sh}, V, I_L, I_D, I_0 represent circuit current, shunt current, work voltage, light current, diode current, dark saturation current, respectively, while q, k, T, n represent the elementary charge, Boltzmann's constant, temperature, ideality factor of the diode, respectively. For the ideal condition, $R_s \to 0$ and $R_{sh} \to \infty$, current density J in the circuit can be expressed as:

$$J = J_{SC} - J_0\left[\exp\left(\frac{qV}{nkT}\right)-1\right] \#(2)$$

The dark saturation current density can be calculated by the standard device condition (AM 1.5G at $J = 0$):

$$J_0 = \frac{J_{SC,\,std}}{\left(\exp\left(\frac{qV_{OC,\,std}}{nkT}\right) - 1\right)} \#(3)$$

where $J_{SC,\,std}$ and $V_{OC,\,std}$ are tested under standard device condition, and the short-circuit current density J_{SC} is obtained from the light absorption represented by the device EQE ($Q(\lambda)$):

$$J_{SC} = \int \frac{q\lambda}{hc}\phi_{sun}(\lambda)Q(\lambda)d\lambda \#(4)$$

where λ, h, c, and ϕ_{sun} are probe wavelength, Planck's constant, speed of light in vacuum, and solar radiation intensity, respectively. Through the above derivation, we can get the $J-V$ curve of the device under specific light radiation represented by Eq. 2, and further obtain its maximum output power point (MPP) P_{max}:

$$P_{max} = \max\,(J \times V) \#(5)$$

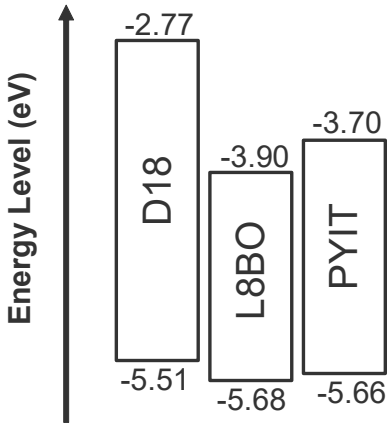

Figure S1. The energy level of D18, L8BO and PYIT.

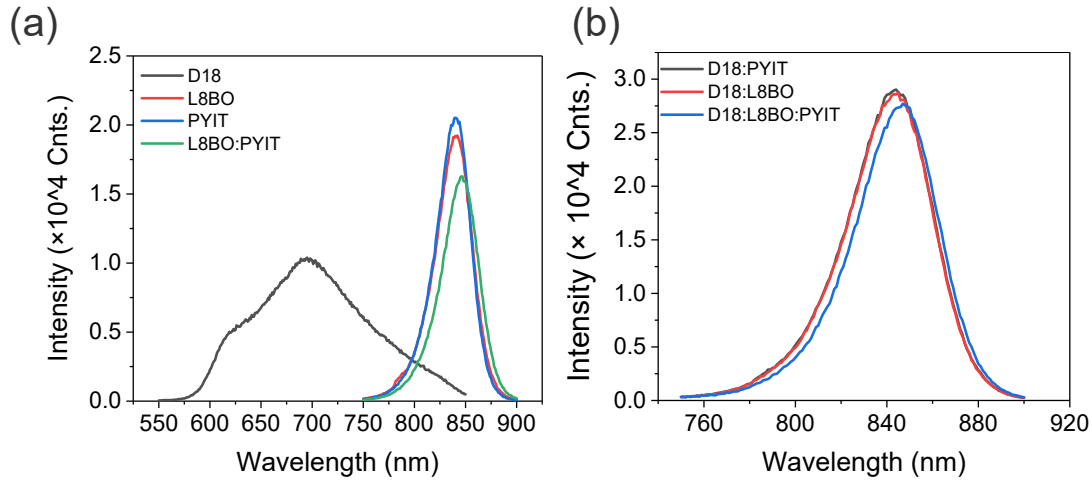

Figure S2. Photoluminescence (PL) of a) neat film and b) blend film (layers on glass). The excitation wavelength was 450 nm laser for donor, 640 nm laser for acceptor and blend film.

Table S1. PL peak and lifetime parameters of neat film and blend film.

	PL-Peak (nm)	τ_{AvAmp} (ns)
D18	695	0.4077
L8BO	840	0.5514
PYIT	840	0.3917
L8BO:PYIT	847	0.5810
D18:PYIT	843	0.1411
D18:L8BO	843	0.1602
D18:L8BO:PYIT	847	0.1661

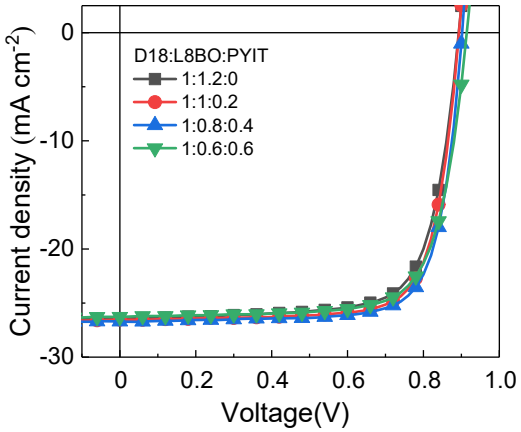

Figure S3. *J–V* characteristics with different D18:L8BO:PYIT ratio.

Table S2. Photovoltaic parameters of OSCs under different ratio of PYIT.

D18:L8BO:PYIT ratio[a]	V_{OC} (V)	J_{SC} (mA cm^{-2})	FF (%)	PCE (%)
1:1.2:0	0.893	26.46	73.77	17.23
1:1:0.2	0.894	26.54	76.06	17.83
1:0.8:0.4	0.901	26.69	76.75	18.16
1:0.6:0.6	0.914	26.28	74.03	17.58

[a] The concentration of polymer donor was 1 mg mL^{-1} in Toluene solution, the solution volume was 115 μL and SVA time was 25 seconds.

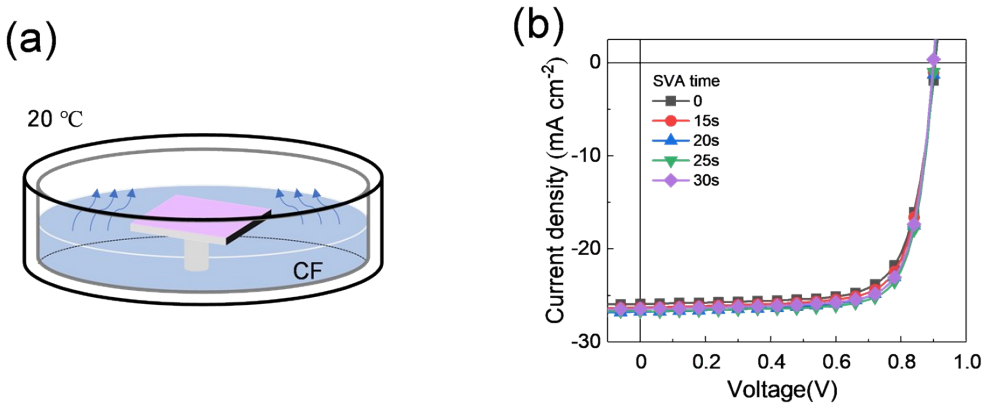

Figure S4. a) Schematic diagram of SVA operation. b) *J–V* characteristics with different SVA time.

Table S3. Photovoltaic parameters of OSCs under different SVA time.

SVA time (S)	V_{OC} (V)	J_{SC} (mA cm^{-2})	FF (%)	PCE (%)
0	0.905	25.92	73.57	17.07
15	0.902	26.30	74.75	17.54
20	0.903	26.76	75.09	17.93
25	0.901	26.69	76.75	18.16
30	0.899	26.47	76.33	17.96

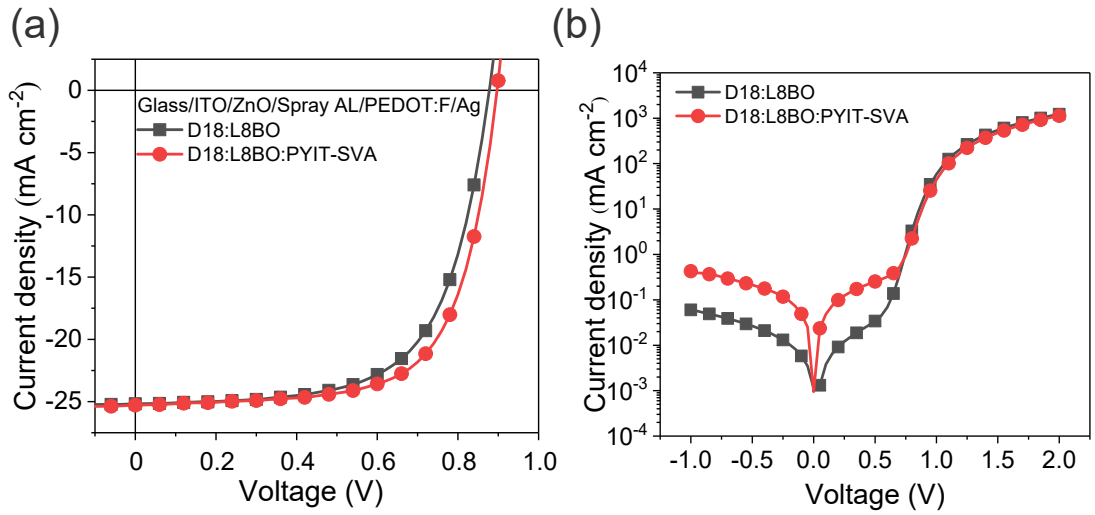

Figure S5. The performance of inverted OSCs with an active layer sprayed in the structure of Glass/ITO/ZnO/Spray Al/PEDOT:F/Ag.

Table S4. Photovoltaic parameters of inverted OSCs with spray-coated active layer.

Active Layer	V_{OC} (V)	J_{SC} (mA cm^{-2})	FF (%)	PCE (%)
D18:L8BO	0.878	25.18	64.46	14.25
D18:L8BO:PYIT-SVA	0.897	25.29	67.34	15.27

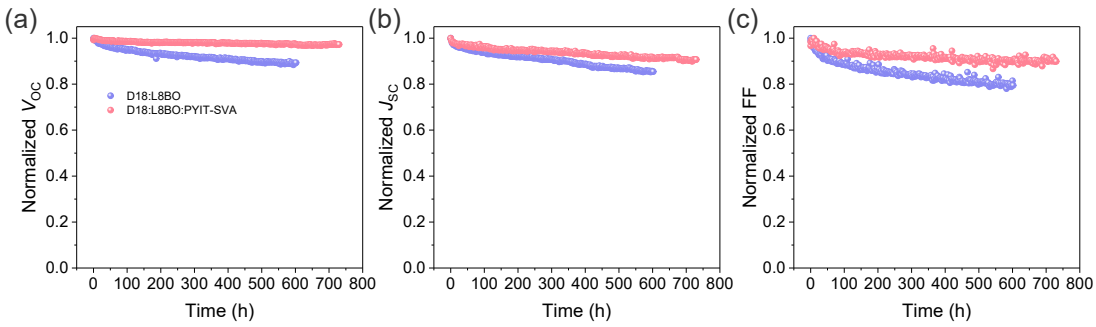

Figure S6. Photostability was assessed under continuous 1 sun illumination at 23 °C in a dry nitrogen atmosphere without encapsulation.

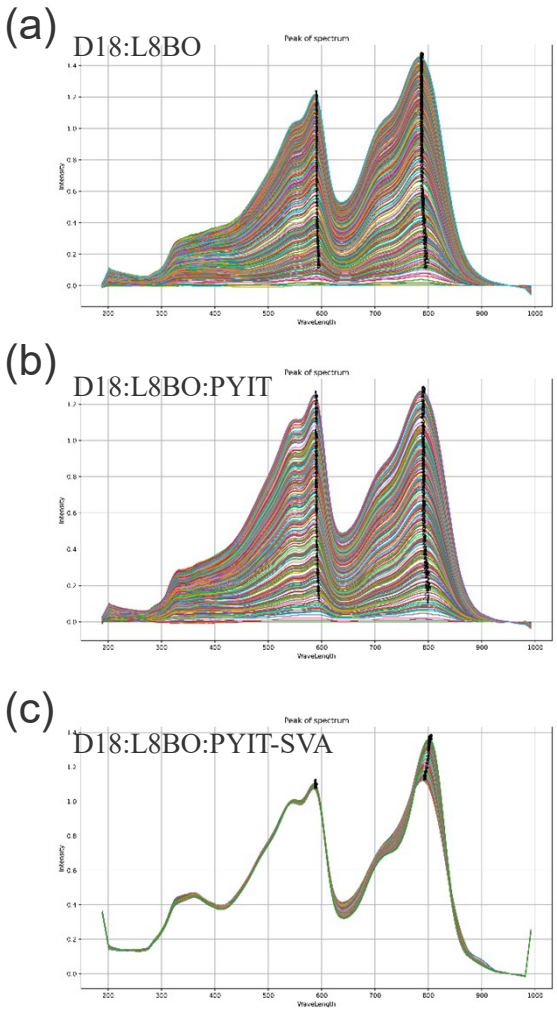

Figure S7. The in-situ peak and intensity tracking for (a) D18:L8BO, (b) D18:L8BO:PYIT and (c) D18:L8BO:PYIT-SVA.

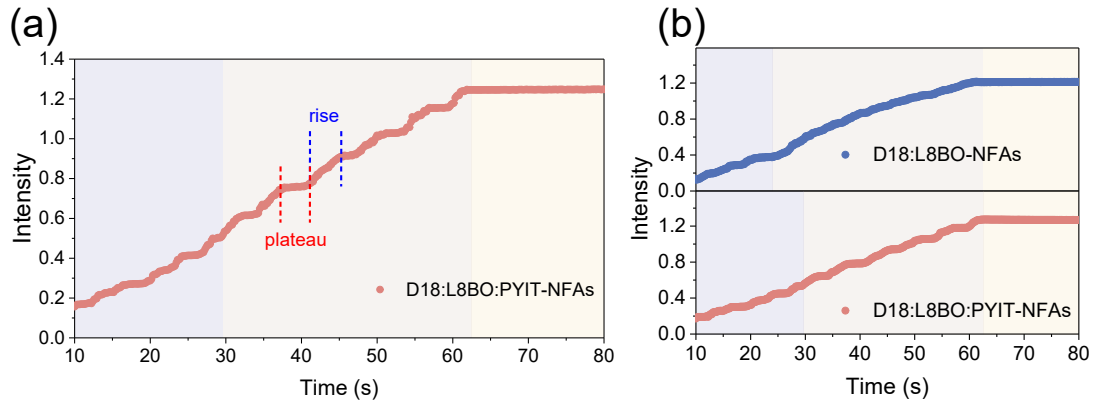

Figure S8. a) Schematic diagram of the division between the rising phase and the plateau phase in in-situ. b) Comparison of binary and ternary systems in in-situ.

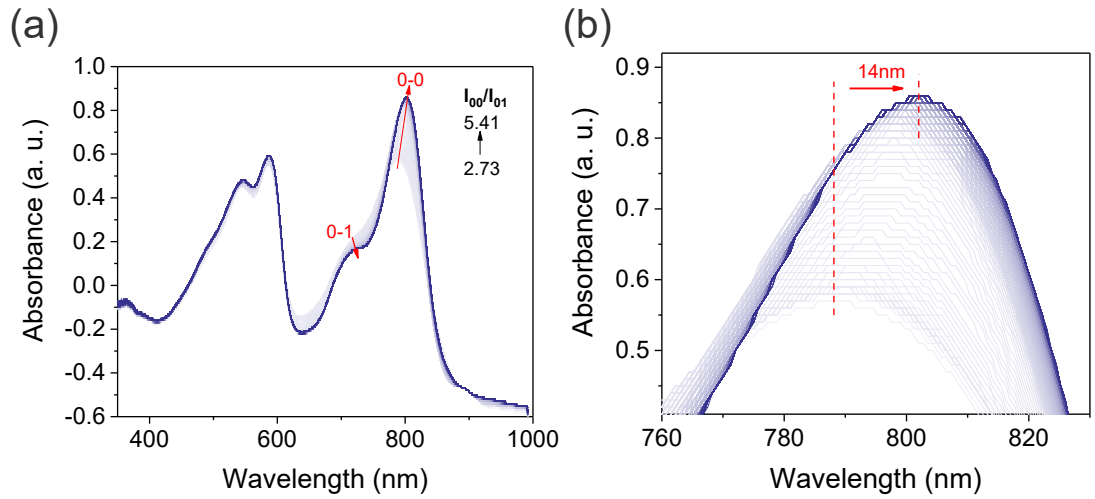

Figure S9. a) The absorption spectrum of the D18:L8BO:PYIT changes with SVA time. b) The change in the acceptor absorption peak.

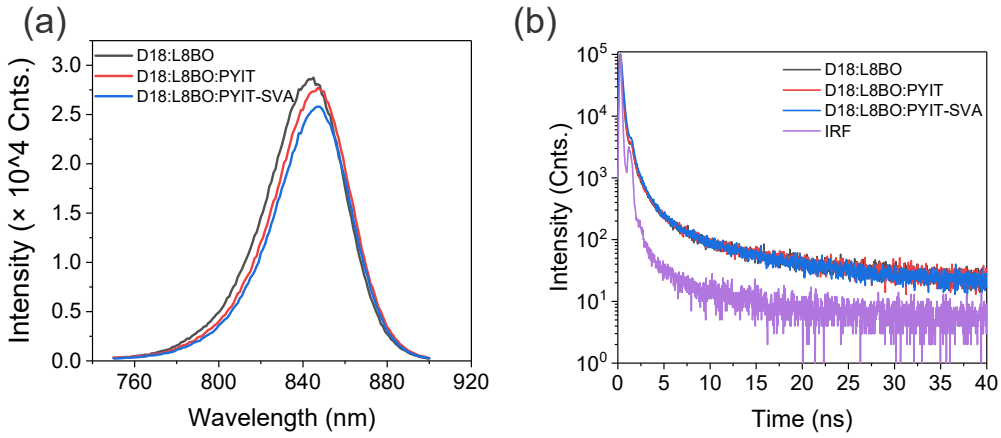

Figure S10. PL and TRPL of blend film (layers on glass).

Table S5. Lifetime parameters of D18:L8BO, D18:L8BO:PYIT and D18:L8BO:PYIT-SVA.

	PL-peak (nm)	τ_{AvAmp} (ns)
D18:L8BO	843	0.1602
D18:L8BO:PYIT	847	0.1661
D18:L8BO:PYIT-SVA	847	0.1936

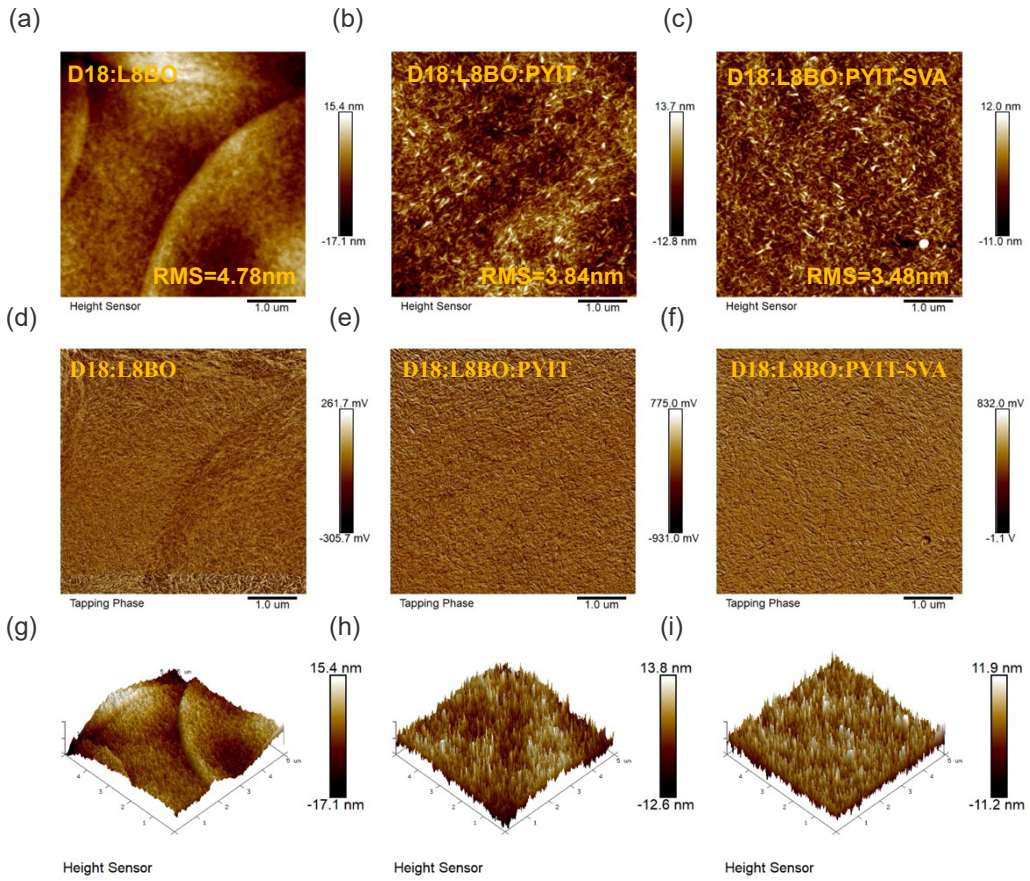

Figure S11. The AFM phase diagrams and 3-D diagrams of all films.

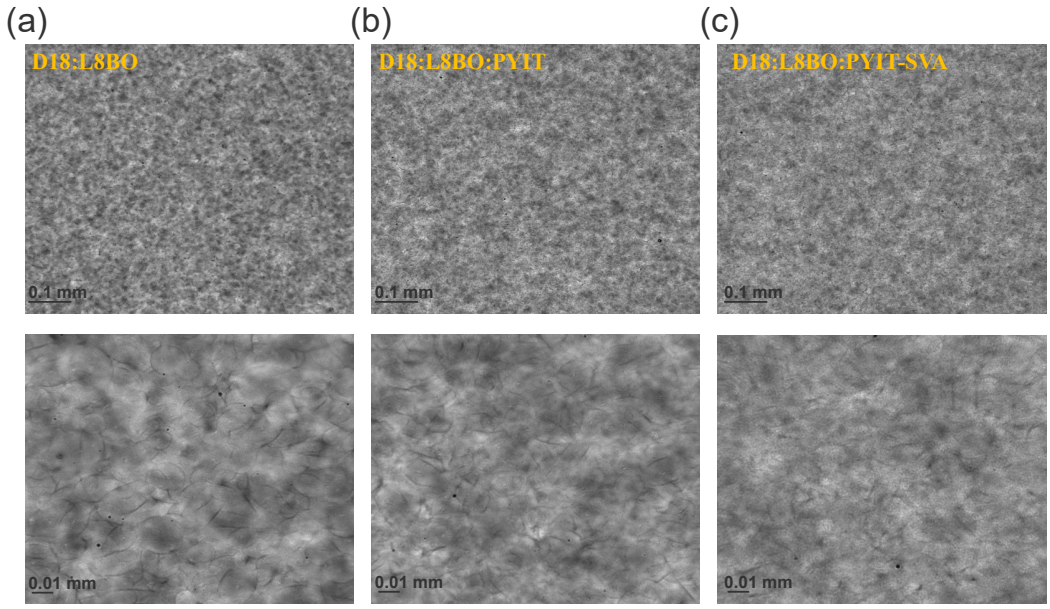

Figure S12. The optical microscope images of all films.

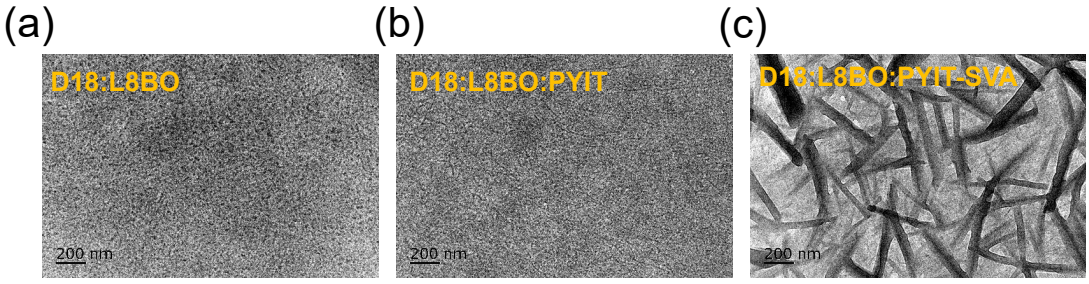

Figure S13. TEM images of the a) D18:L8BO, b) D18:L8BO:PYIT and c) D18:L8BO:PYIT-SVA active layers.

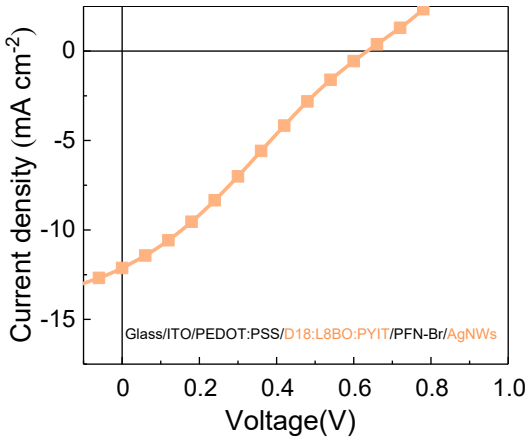

Figure S14. *J–V* characteristics of conventional OSCs (ITO/PEDOT:PSS/sprayed D18:L8BO:PYIT/PFN-Br/sprayed AgNWs) with sprayed AgNWs top electrode.

Table S6. Photovoltaic parameters of conventional OSCs fabricated with sprayed AgNWs top electrode.

V_{OC} (V)	J_{SC} (mA cm^{-2})	FF (%)	PCE (%)
0.64	12.13	27.28	2.10

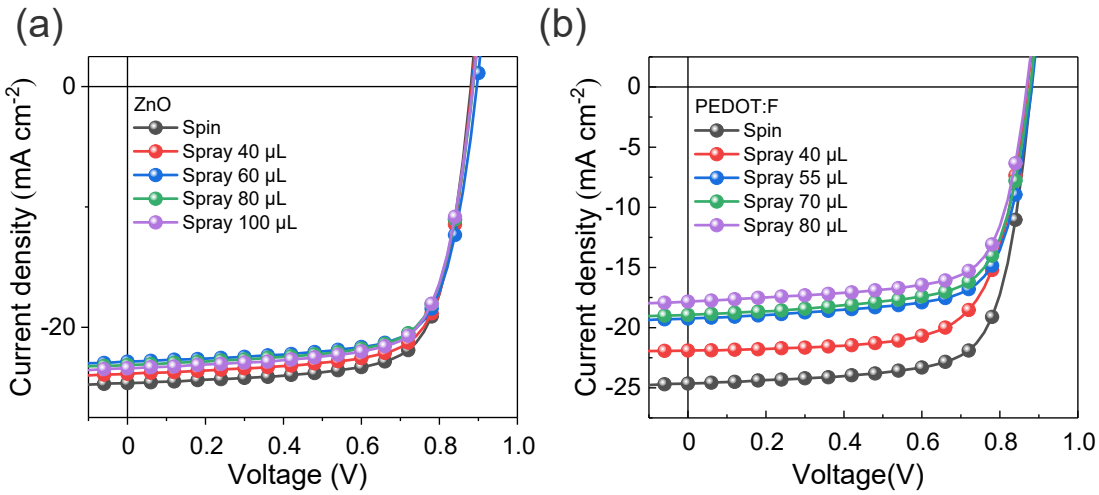

Figure S15. The performance of a) Spray B and b) Spray C in the structure of Glass/ITO/ZnO/D18:L8BO:PYIT/PEDOT:F/Ag.

Table S7. Photovoltaic parameters of Spray B and Spray C devices.

		Volume (µL)	V_{OC} (V)	J_{SC} (mA cm^{-2})	FF (%)	PCE (%)
ZnO	Spin	35	0.88	24.65	72.66	15.77
	Spray	40	0.88	23.87	72.82	15.35
		60	0.90	22.86	72.56	14.86
		80	0.89	23.14	72.04	14.77
		100	0.89	23.41	71.97	14.92
PEDOT:F	Spin	35	0.88	24.65	72.66	15.77
	Spray	40	0.87	21.90	70.29	13.41
		55	0.88	19.25	71.35	12.11
		70	0.88	18.94	70.11	11.65
		80	0.87	17.83	71.03	11.00

Table S8. Photovoltaic parameters of OSCs from the spraying of the active layer to fully spray coating.

	V_{OC} (V)	J_{SC} (mA cm^{-2})	$J_{SC, EQE}$ (mA cm^{-2})	FF (%)	PCE (%)
Spray A	0.89	24.28	23.91	73.22	15.91
Spray B	0.88	23.87	22.86	72.82	15.35
Spray C	0.87	21.90	20.81	70.29	13.41
Spray D	0.88	19.31	18.83	68.90	11.72
Spray E	0.84	19.80	19.19	45.20	7.55

Table S9. The optical and electrical parameters of the AgNWs and AgNWs@ZnO electrodes.

Resistance (Ω sq^{-1})	Transmittance (%)	Resistance (Ω sq^{-1})	Transmittance (%)
Spray AgNWs@ZnO		Spray AgNWs	
28.91	91.65	12.5	86.75
30.86	92.42	15.71	88.94
46.43	93.84	16.6	89.33
48.77	93.77	20.97	88.05
54.79	94.12	23.54	90.31
60.81	94.94	24.62	87.87
68.98	95.32	24.87	87.03
84.23	96.55	25.32	91.11
95.7	96.66	26.86	89.2
98.2	96.04	27.6	92.01
133.5	96.36	32.02	92.94
134.5	95.76	38.81	91.63
195.9	97.61	42.04	92.95
231.5	97.2	62.3	92.65
		63.73	92.43
		84.94	93.32
		95.74	92.71
		101.3	93.48

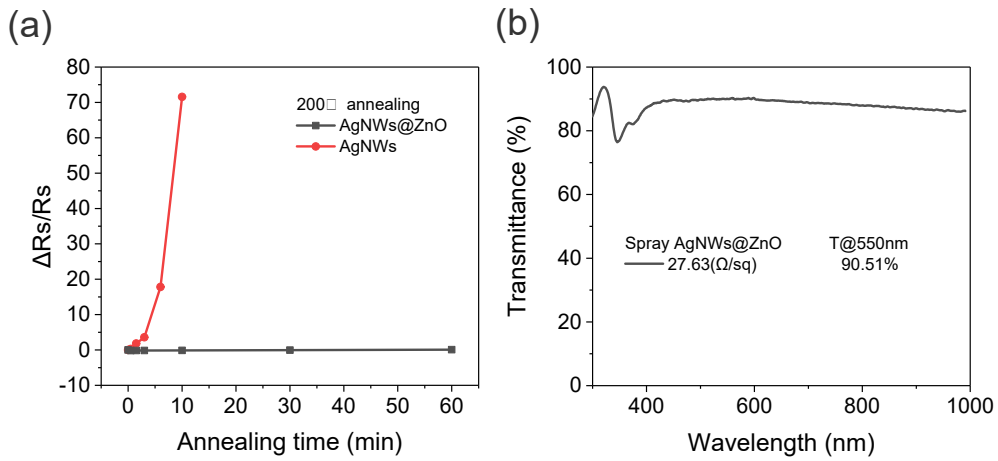

Figure S16. The a) heat resistance and b) transmission spectrum of sprayed AgNWs@ZnO film.

Table S10. The sheet resistance of the AgNWs and AgNWs@ZnO electrodes during the 200 ℃ annealing process.

	Annealing time (min)	Resistance (Ω sq^{-1})	ΔRs/Rs
AgNWs	0	30.32	0.00
	0.5	39.5	0.30
	1.5	85.7	1.83
	3	138.5	3.57
	6	570.5	17.82
	10	2200	71.56
AgNWs@ZnO	0	42.82	0.00
	0.5	35.18	-0.18
	1.5	36.24	-0.15
	3	36.31	-0.15
	10	37.47	-0.12
	30	41.12	-0.04
	60	46.73	0.09

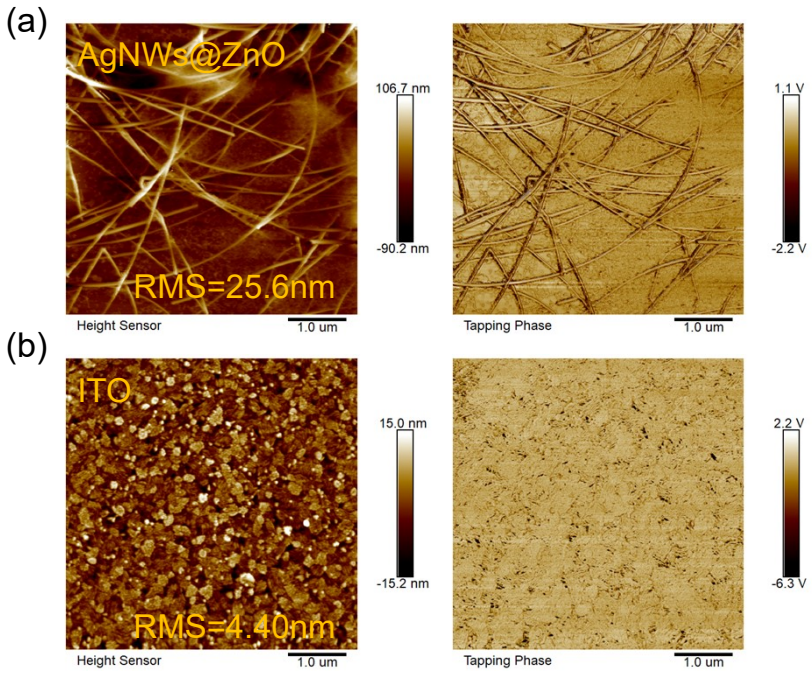

Figure S17. AFM images of a) AgNWs@ZnO and b) ITO.

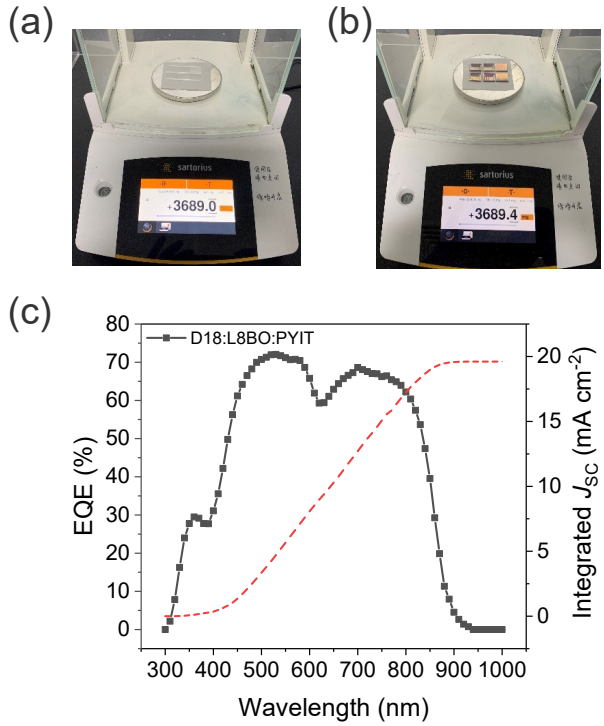

Figure S18. The quality of the glass a) without and b) with all-spray OSCs. c) EQE curves of the optimal all-spray OSCs.

Table S11. Photovoltaic parameters of the optimal OSCs fabricated with all-spray coating.

V_{OC} (V)	J_{SC} (mA cm^{-2})	$J_{SC,\ EQE}$ (mA cm^{-2})	FF (%)	PCE (%)	Δm (mg)	ρ=m/s (g m^{-2})	Power-to-weight ratio (W g^{-1})
0.84	19.8	19.609	45.2	7.55	0.06667	0.2963	254.8125

Calculation of power-to-weight ratio

Six independent OSCs with a size of 1.5 cm × 1.5 cm were fabricated on a glass substrate. The weights of the glass with and without the independent OSCs were measured, and the difference in quality was the mass of the six independent devices, as shown in Figure S13a-b.

The total weight of these six independent devices is 0.4 mg. The formula for calculating the areal density is

$$\rho = \frac{m}{s} = \frac{0.0004\ g}{6 \times 1.5 \times 1.5 \times 10^{-4}\ m^2} = 0.2963\ g\ m^{-2}$$

Power density is calculated by multiplying the incident power (P_{in}) and PCE:

$$P = P_{in} \times PCE = 1000\ W\ m^{-2} \times 7.55\% = 75.5\ W\ m^{-2}$$

The power-to-weight ratio:

$$Power - to - weight\ ratio = \frac{P}{\rho} = \frac{75.5\ W\ m^{-2}}{0.2963\ g\ m^{-2}} = 254.8\ W\ g^{-1}$$

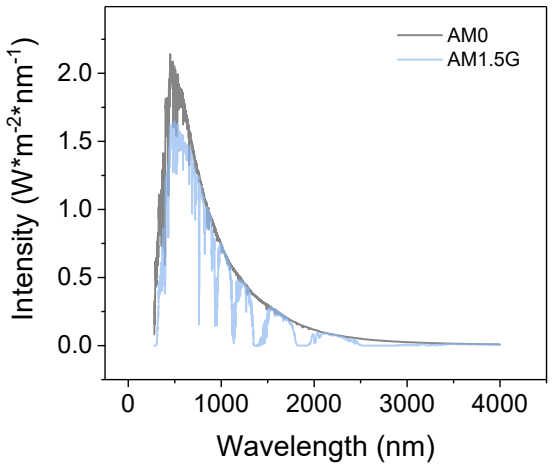

Figure S19. Solar irradiation data under AM0 and AM1.5G conditions.

Table S12. The photovoltaic simulation parameters, annual electricity generation capacity and corresponding power-to weight ratio under AM0 conditions in the most ideal scenario.

J_{SC} (mA cm^{-2})	V_{OC} (V)	FF (%)	PCE (%)	P_in (mW cm^{-2})	P_out (mW cm^{-2})	Energy yield (kWh m^{-2} year^{-1})	Power-to-weight ratio (W g^{-1})
23.27	0.8491	82.95	17.56	93.37	16.39	1435.8	592.65

The simulation data were obtained through solar irradiation under AM0 conditions, the *J-V* curve and EQE integral curve of the device. It is assumed that in the most ideal case and the recombination loss is not considered.

Table S13. Summary of the device structure and efficiency of OSCs with spray-coated active layers reported in the literature.

Year	Device Structure	PCE (%)	Ref.
2007	Glass/ITO/PEDOT:PSS/P3HT:PCBM/Ca/Al	2.83	2
2015	ITO/ZnO /PTB7:PC71BM /MoO3 /Ag	7.62	3
2019	Ag/PFN/PTB7:PC71BM or PBDB-T:IT-M/PEDOT:PSS	8.06	4
2020	Glass/ITO/PEDOT:PSS/PTB7-Th:FOIC/PDINO/Al	9.45	5
2020	Glass/ITO/PEDOT:PSS/PBDB-T-2Cl:IT-4F/ZnO/Al	12.29	6
2021	Glass/ITO/PEDOT:PSS/PM6:N3/PDINN/Ag	15.98	7
2023	Glass/ITO/ZnO/PM6:DTY6/MoOx/Ag	14.1	8
2023	Glass/ITO/PEDOT:PSS/PM6:L8BO/ZnO/Al	13.96 15.78	9
2023	Glass/ITO/PEDOT:PSS/PM6: BTP-eC9/PNDIT-F3N/Ag	17.13	10
2025	Glass/ITO/PEDOT:PSS/PM6:DTY6:L8BO/PFN-Br/Ag	15.39	11
2026	**Glass/ITO/PEDOT:PSS/D18:L8BO:PYIT/PFN-Br/Ag**	**18.27**	**This work**

Table S14. Summary of the device structure and efficiency of PV technologies with hight Power-to-weight ratio reported in the literature.

PV technologies	Year	Device Structure	PCE (%)	Power-to-weight ratio (W g^{-1})	Ref.
Organic	2021	PET/PH1000/PEDOT:PSS(4083)/ D18-Cl:Y6:PC71BM/PFNDI-Br/Ag	15.5	32.07	12
	2022	tPI/ITO/PEI-Zn/PM6:Y6/MoO3/Ag	15.8	33.8	13
	2023	PI/Ag/PCP-2F-Li/PEDOT:PSS/PM6:L8- BO/Bis-FIMG/Au/Ag/TeO2	17.32	39.72	14
	2024	Parylene/ITO/MoO3/PEDOT:PSS/ PM6:L8-BO/PDINN/Ag	17.01	39.3	15
	2024	Parylene/ITO/ZnO(IZO)/PM6:L8-BO:BTP-eC9/MoO3/Ag	17	40.4	16
	2025	PH1000/Al 4083/PM6:Y6/PFN-Br/Ag	11.6	109.4	17
	2026	**AgNWs@ZnO/ZnO/D18:L8BO:PYIT/PEDOT:F/AgNWs**	**7.55**	**254.8**	**This work**
GaAs	2022	Ga0.51In0.49P/GaAs/Ga0.73In0.27As	30.9	3	18
Quantum Dots	2020	PET/parylene/graphene/oCVD PEDOT/Pbs-EDT/Pbs-TBAI/LiF/Al	7.1	12.3	19
Perovskite	2017	PET/ITO/NiOx/Perovskite/C60/Bis-C60/Ag	14.19	23.26	20
	2019	PEN/AgNWs/PH1000/Al4083/ Perovskite/PC61BM/Al	15.18	29.4	21
	2022	Parylene/ITGZO/PTAA/Perovskite/PCBM/BCP/Cu	20.20	30.3	22

References

1 P. Schilinsky, C. Waldauf and C. J. Brabec, *Appl. Phys. Lett.*, 2002, **81**, 3885–3887.

2 D. Vak, S.-S. Kim, J. Jo, S.-H. Oh, S.-I. Na, J. Kim and D.-Y. Kim, *Appl. Phys. Lett.*, 2007, 91.

3 D. Zheng, J. Huang, Y. Zheng and J. Yu, *Org. Electron.*, 2015, **25**, 275–282.

4 A. Liu, W. Zheng, X. Yin, J. Yang, Y. Lin, W. Cai, X. Yu, Q. Liang, Z. He, H. Wu, Y. Li, F. Zhang and L. Hou, *ACS Appl. Mater. Interfaces*, 2019, **11**, 10777–10784.

5 K. Chang, Y. Li, G. Du, M. Zhong, P. Yang, Y. Zhu, F. He, B. Mi, X. Zhao and W. Deng, *ACS Appl. Mater. Interfaces*, 2020, **12**, 27405–27415.

6 J. Cheng, S. Wang, Y. Tang, R. Hu, X. Yan, Z. Zhang, L. Li and Q. Pei, *Solar RRL*, 2020, **4**, 1900458.

7 K. Chang, Y. Li, H. Xia, J. Chang, B. Yu, G. Du, P. Yang, X. Zhao, B. Mi, W. Huang and W. Deng, *ACS Appl. Mater. Interfaces*, 2021, **13**, 56375–56384.

8 E. L. K. Spooner, E. J. Cassella, J. A. Smith, T. E. Catley, S. Burholt and D. G. Lidzey, *ACS Appl. Mater. Interfaces*, 2023, **15**, 39625–39635.

9 L. Sang, X. Chen, J. Fang, P. Xu, W. Tian, K. Shui, Y. Han, H. Wang, R. Huang, Q. Zhang, Q. Luo and C. Ma, *Adv. Funct. Mater.*, 2023, **33**, 2304824.

10 K. Chang, B. Yu, L. Liu, D. Fang, X. Zhao, B. Mi, W. Huang and W. Deng, *Adv. Mater. Technol.*, 2023, **8**, 2201921.

11 Q. Wang, K. An, X. Cui, X. Jiang, X. Kang, J. Qi, X. Hui, J. Wu, X. Zhang, Z. Yin, W. Meng, Y. Jiang, Y. Zhou, K. Yan, L. Ying, S. V. Roth and N. Li, *EES Solar*, 2025, **1**, 847–856.

12 W. Song, K. Yu, E. Zhou, L. Xie, L. Hong, J. Ge, J. Zhang, X. Zhang, R. Peng and Z. Ge, *Adv. Funct. Mater.*, 2021, **31**, 2102694.

13 S. Xiong, K. Fukuda, S. Lee, K. Nakano, X. Dong, T. Yokota, K. Tajima, Y. Zhou and T. Someya, *Advanced Science*, 2022, **9**, 2105288.

14 X. Zheng, L. Zuo, K. Yan, S. Shan, T. Chen, G. Ding, B. Xu, X. Yang, J. Hou, M. Shi and H. Chen, *Energy Environ. Sci.*, 2023, **16**, 2284–2294.

15 D. Zhang, Y. Ji, Y. Cheng, X. Liu, Z. Xia, X. Liu, X. Liu, X. Yang and W. Huang, *J. Mater. Chem. A Mater.*, 2024, **12**, 15099–15105.

16 X. Liu, Y. Ji, Z. Xia, D. Zhang, Y. Cheng, X. Liu, X. Ren, X. Liu, H. Huang, Y. Zhu, X. Yang, X. Liao, L. Ren, W. Tan, Z. Jiang, J. Lu, C. McNeill and W. Huang, *Advanced Science*, 2024, **11**, 2402158.

17 J. Chang, Z. Zheng, Q. Jiang and D. Liu, *ACS Appl. Mater. Interfaces*, 2025, **17**, 21552–21559.

18 J. Schön, G. M. M. W. Bissels, P. Mulder, R. H. van Leest, N. Gruginskie, E. Vlieg, D. Chojniak and D. Lackner, *Progress in Photovoltaics: Research and Applications*, 2022, **30**, 1003–1011.

19 M. M. Tavakoli, M. H. Gharahcheshmeh, N. Moody, M. G. Bawendi, K. K. Gleason and J. Kong, *Adv. Mater. Interfaces*, 2020, **7**, 2000498.

20 H. Zhang, J. Cheng, D. Li, F. Lin, J. Mao, C. Liang, A. K. -Y. Jen, M. Grätzel and W. C. H. Choy, *Advanced Materials*, 2017, **29**, 1604695.

21 S. Kang, J. Jeong, S. Cho, Y. J. Yoon, S. Park, S. Lim, J. Y. Kim and H. Ko, *J. Mater. Chem. A Mater.*, 2019, **7**, 1107–1114.

22 J. Wu, P. Chen, H. Xu, M. Yu, L. Li, H. Yan, Y. Huangfu, Y. Xiao, X. Yang, L. Zhao, W. Wang, Q. Gong and R. Zhu, *Sci. China Mater.*, 2022, **65**, 2319–2324.